Novel Sulfur-Tolerant Anodes for Solid Oxide Fuel Cells

Final Report

Reporting Period: October 1, 2004 to December 31, 2008

DOE Contract No.: DOE - DE-FC26-04NT42219
DOE Project Manager: Dr. Briggs White

Prepared by

Lei Yang and Meilin Liu

Center for Innovative Fuel Cell and Battery Technologies
School of Materials Science and Engineering
Georgia Institute of Technology
Atlanta, GA 30332-0245

Report Issued: March 2009

DISCLAIMER

ABSTRACT

One of the unique advantages of SOFCs over other types of fuel cells is the potential for direct utilization of hydrocarbon fuels (it may involve internal reforming). Unfortunately, most hydrocarbon fuels contain sulfur, which would dramatically degrade SOFC performance at parts-per-million (ppm) levels. Low concentration of sulfur (ppm or below) is difficult to remove efficiently and cost-effectively. Therefore, knowing the exact poisoning process for state-of-the-art anode-supported SOFCs with Ni-YSZ cermet anodes, understanding the detailed anode poisoning mechanism, and developing new sulfur-tolerant anodes are essential to the promotion of SOFCs that run on hydrocarbon fuels.

The effect of cell operating conditions (including temperature, H_2S concentration, cell voltage/current density, etc.) on sulfur poisoning and recovery of nickel-based anode in SOFCs was investigated. It was found that sulfur poisoning is more severe at lower temperature, higher H_2S concentration or lower cell current density (higher cell voltage). *In-situ* Raman spectroscopy identified the nickel sulfide formation process on the surface of a Ni-YSZ electrode and the corresponding morphology change as the sample was cooled in H_2S-containing fuel. Quantum chemical calculations predicted a new S-Ni phase diagram with a region of sulfur adsorption on Ni surfaces, corresponding to sulfur poisoning of Ni-YSZ anodes under typical SOFC operating conditions. Further, quantum chemical calculations were used to predict the adsorption energy and bond length for sulfur and hydrogen atoms on various metal surfaces. Surface modification of Ni-YSZ anode by thin Nb_2O_5 coating was utilized to enhance the sulfur tolerance.

A multi-cell testing system was designed and constructed which is capable of simultaneously performing electrochemical tests of 12 button cells in fuels with four different concentrations of H_2S. Through systematical study of state-of-the-art anode-supported SOFC button cells, it is seen that the long-term sulfur poisoning behavior of those cells indicate that there might be a second-stage slower degradation due to sulfur poisoning, which would last for a thousand hour or even longer. However, when using G-18 sealant from PNNL, the 2^{nd} stage poisoning was effectively prohibited.

TABLE OF CONTENTS

INTRODUCTION

One of the unique advantages of SOFCs over other types of fuel cells is the fuel flexibility. SOFCs have the potential of direct utilization of hydrocarbon fuels. Compared with pure hydrogen, hydrocarbon fuels have higher energy density and are readily available and easier to transport and store based on current infrastructure[1-3]. To use them, hydrocarbon fuels are reformed externally or internally into CO and H_2 on catalysts such as nickel. However, one problem with all hydrocarbon fuels is that they all contain contaminants such as sulfur compounds[4]. For example, sulfur concentration in pipeline natural gas is usually several ppm by volume while sulfur concentration in liquid fuels such as gasoline, jet propellant and diesel could be as high as ~100-1000 ppm by volume. The sulfur compounds would transform into gaseous hydrogen sulfide (H_2S) in the reforming process and readily poison the nickel-based anode for SOFCs, leading to dramatic reduction in cell performance and operational life.

Although considerable efforts have been devoted to the development of sulfur-tolerant anode materials, a detailed understanding of the sulfur poisoning process and its mechanism is still lacking, and there is no anode material that is both sulfur-tolerant and compatible with current cell materials/fabrication techniques. Further, knowing the exact poisoning process for state-of-the-art cells with Ni-YSZ supporting anodes is essential for the promotion of SOFCs that run on hydrocarbon fuels.

The current project focuses on (i) studying the poisoning process of Ni-based anodes by H_2S in SOFCs under different operation conditions (ii) investigating the sulfur poisoning mechanism for the Ni-based anode via experiments and theoretical calculations, (iii) establishing scientific principles that may guide the selection of candidate sulfur resistant anode materials and developing new anode materials and/or architectures that provide enhanced sulfur tolerance (iv) characterizing both the immediate and the slow sulfur poisoning process for state-of-the-art SOFC button cells with a anode-supported structure under various operating conditions.

EXECUTIVE SUMMARY

Quantum chemical calculations and Raman spectroscopy have been used to investigate into the detailed mechanisms for sulfur poisoning of nickel-based anodes under typical SOFC operating conditions. We have successfully predicted a new S-Ni phase diagram for a region of sulfur adsorption on Ni surfaces, corresponding to sulfur poisoning of Ni-YSZ anodes under typical SOFC operating conditions. We have also predicted the adsorption energy and bond length for sulfur and hydrogen atoms on various metal surfaces. Surface modification of a Ni-YSZ anode by a thin Nb_2O_5 coating was utilized to enhance the sulfur tolerance of Ni-YSZ anodes.

Formation of nickel sulfides on the surface of a Ni-YSZ anode was identified using *in situ* Raman spectroscopy as the sample was cooled in a H_2S-containing fuel, suggesting that sulfur poisoning was caused by the adsorption of sulfur atoms on nickel surface, not by the formation of nickel sulfides as reported in previous studies.

We have further studied the effects of cell operating conditions (including temperature, H_2S concentration, cell voltage/current density, etc.) on sulfur poisoning and recovery of nickel-based anode in SOFCs. Generally, sulfur poisoning is more severe at lower temperature, higher H_2S concentration or lower cell current density (higher cell voltage).

Finally, we have characterized sulfur poisoning behavior of state-of-the-art anode-supported SOFC button cells under various operating conditions using our 12-cell testing system, including the concentration of H_2S and cell current density. The effect of sealant on 2^{nd} stage poisoning behavior was also observed.

EXPERIMENTAL

Operation conditions

The cell current at a constant voltage was monitored continuously when H_2S gas (at the ppm level) was introduced and removed from the fuel flow under different conditions (temperature, H_2S concentration and cell current density/voltage, etc.). The impedance responses of the cell under open-circuit conditions were also measured in fuels with and without H_2S to determine the contributions from the electrolyte and different interfaces.

Mechanism study

The sulfur–anode interaction was investigated by characterizing the chemical and structural changes on the surface of dense Ni-YSZ composites. This includes *in-situ* Raman spectroscopy, in which the Raman signal and structure at elevated temperatures were obtained on a real-time basis when H_2S was introduced and removed from the Raman cell. The results from in-situ Raman spectroscopy were also correlated with other ex-situ techniques such as SEM, EDX, and XRD, etc. to study the sulfur-anode interaction.

In theoretical analysis, quantum chemical calculations with thermodynamic correction were used to predict the interactions between H_2S-contaminated hydrogen fuel and Ni surfaces under SOFC operation conditions. The vibrational frequencies and modes of several nickel sulfides were computed using finite displacement approach to assist the interpretation of Raman spectra obtained from experiments. The electronic structures of these sulfides were also calculated and correlated with the poisoning behavior.

Novel anode with sulfur tolerance

Quantum chemical calculations were used to predict the adsorption energy and bond length for sulfur and hydrogen atoms on various metal surfaces. The results were used to predict sulfur tolerance and anode activity toward electrochemical oxidation of H_2 fuel for those different materials.

The surfaces of Ni-YSZ anodes were modified with a thin film of other materials to improve the sulfur tolerance. Fuel cells with dense Ni-YSZ anodes were fabricated using a co-sintering method in a reducing atmosphere. A thin film of Nb_2O_5 was then deposited on the anode surface by sputtering. The power output and the interfacial impedance response were recorded as a function of time upon exposure to hydrogen with or without 50 ppm H_2S. Further, quantum chemical calculations were used to predict the thermodynamic stability, electronic structure, and vibrational frequencies for niobium

oxides and sulfides, which helped to explain the origin of the enhanced sulfur tolerance for Ni-YSZ cermet anodes modified using a thin coating of niobium oxide.

Multi-cell testing

A multi-cell testing system was designed and constructed in our lab, consisting of a high temperature furnace, a gas distribution system, and a 12-channel electrochemical testing station. It had been carried out to evaluate both the short-term and the long-term sulfur poisoning behavior for state-of-the-art anode-supported SOFC button cells. Initially, Aremco sealant (Ceramabond® 552VFG) was employed in commercial cells with LSM and LSCF based cathode. Then G-18 glass sealant (from PNNL) was investigated to obtain more information about the poisoning behaviors of these cells

RESULTS AND DISCUSSIONS

Effect of cell operating conditions on sulfur poisoning and recovery

Sulfur poisoning of the Ni-YSZ cermet anode for SOFCs consists of two stages. The first is a rapid degradation within a few minutes that causes the majority of the decrease in performance, followed by a gradual degradation that occurs over several hours or even days. The extent of degradation is influenced by cell voltage (or, alternatively, the cell current density). The higher the cell current density (or the lower the cell operating voltage), the lower the extent of sulfur poisoning. The recovery of the poisoned anode can be realized by continuous flowing of sulfur-free fuel, and the recovery is faster when the cell current density is higher (Figure 1(a)). Impedance studies show that the degradation in cell performance was caused by a large increase in anode interfacial resistance while there is no significant change in bulk resistance (Figure 1(b)). The anode interfacial resistance increases as H_2S concentration increases (Figure 1(c)). Correspondingly, at certain temperature and cell voltage, the extent of sulfur poisoning increases with increasing H_2S concentration until saturation is reached. With the same concentration of H_2S, the extent of sulfur poisoning increases dramatically with decreasing temperature. The lowest tolerable H_2S level also decreases dramatically with decreasing temperature (Figure 1(d)).

Sulfur poisoning mechanism of Ni-YSZ

In-situ Raman spectroscopy experiments show no sign of conventional nickel sulfide formation on the surface of the Ni-YSZ composite and there is also no significant change in surface morphology when the sample is exposed to fuels containing 50 ppm H_2S at high temperatures (>~500 ^oC). However, when the Ni-YSZ composite sample was

cooled down in H_2S-containing fuels, conventional nickel sulfide (e.g., Ni_3S_2) gradually forms on the Ni surface, accompanied by dramatic change in surface morphology (Figures 2(a) and 2(b)). When the sample is cooled down completely, the surface of Ni particles is full of ball-like and/or edge-like structures as shown in Figures 2(c) and 2(e). The Raman spectra give sharp peaks corresponding to Ni_xS_y. The distribution of sulfur on the Ni-YSZ composite is confined to the Ni region (Figures 2(e) – 2(f)). This preliminary study indicates that the fundamental reasoning for sulfur poisoning is most likely sulfur adsorption on the anode. Cooling of the anode in H_2S-containing fuel (even in the ppm range) should be avoided since it causes formation of bulk nickel sulfides and irreversible morphology changes.

Shown in Figure 3 is a new S-Ni phase diagram constructed from quantum chemical calculations with thermodynamic corrections. This phase diagram suggests that a clean Ni surface (in the white region) will first adsorb sulfur atoms when exposed to small amount of H_2S, crossing the blue line and entering the blue (middle) region. The surface coverage of nickel by sulfur increases as the temperature is reduced until the surface is completely covered by sulfur (approaching the red line between the blue and the yellow region) before the formation of Ni_3S_2 (in the yellow region). The blue region can not be predicted directly from the classical thermodynamic database and, thus, is missing from the existing S-Ni phase diagram[5]. The important implication of the calculated phase diagram is that it can be used to accurately predict the conditions to avoid sulfur poisoning (in the white region) and to explain existing measurements[6]. These results also suggest that sulfur poisoning is due to the adsorption of sulfur atoms on the nickel surface, which blocks active sites for fuel oxidation[7].

Listed in Table 1 are the Raman frequencies of 4 nickel sulfide species (i.e., Ni_3S_2, NiS, Ni_3S_4, and NiS_2) determined from DFT calculations as well as from Raman measurements. The computed vibrational frequencies are generally in good agreement with Raman spectra obtained by experiments (with deviation of less than <10 %) and can be used to identify nickel sulfides in our sulfur poisoning studies. The significance of the theoretical calculations is that previous studies on the nickel sulfide Raman spectra often contradicts one another, which makes it impossible to use any of them as a reliable reference.

Development of sulfur-resistant anode

Quantum chemical calculations have been used to estimate the adsorption energy of sulfur species and hydrogen on different transition metal surfaces. Figure 4 shows the normalized adsorption energy for H_2S and H_2 on various transition metals surfaces

obtained from quantum chemical calculations. According to the study, the adsorption of sulfur on metals such as Ag, Cu, V, Cr and Mo is significantly weaker compared with Ni, suggesting possible sulfur tolerance for these materials.

Shown in Figure 5 are the electrochemical measurements on cells having a structure of Pt/YSZ/dense Ni-YSZ with or without Nb_2O_5 coating in dry H_2 at 700 ºC. In Figure 5(a), the increased power density (from 23 to 49 mW/cm^2 for the cell with a Nb_2O_5 coating) indicates that Nb_2O_5 enhanced cell performance after (partially) reduced in H_2. This is also supported by the impedance data shown in Figure 5(b); the interfacial resistance decreased from 15 for the cell without Nb_2O_5 coating to 7 $\Omega \cdot cm^2$ for the cell with a Nb_2O_5 coating. Shown in Figure 5 (c) is the stability of the cell with a Nb_2O_5 coated anode exposed to 50ppm H_2S at 700 °C. The current density dropped slightly as H_2S was first introduced, but quickly recovered to the same value as in H_2 fuel. The cell with Nb_2O_5 coating showed stable performance in fuel with 50 ppm H_2S for 12 h.

Figures 6 (a) to (c) show the Raman spectrum for niobium oxide (Nb_2O_5) after heat treatment in fuels with and without H_2S. Upon heat treatment in H_2, Nb_2O_5 was reduced to NbO_2 as shown in Figure 6(a). In comparison, if Nb_2O_5 was exposed to fuels containing 100 ppm H_2S at similar temperatures, the Raman peaks that corresponds to NbS_2 were identified on the surface of NbO_2, as shown in Figure 6(b). Figure 6(d) shows the results of the density of state (DOS) calculation for niobium oxide (NbO_2) and niobium sulfide (NbS_2). The results indicate that there are no obvious band gaps around the Fermi level for both NbO_2 and NbS_2, which means that NbS_2 formed is still conductive just like NbO_2. In addition, NbO_2 and NbS_2 have similar DOS distribution indicates that both probably have similar catalytic abilities. Based on the information, it is concluded that the enhanced sulfur tolerance for niobium oxide coated Ni-YSZ is due to the transition of the surface from niobium oxide to niobium sulfide, i.e., from NbO_2 to NbS_2, which do not lead to negative impact on the electronic and catalytic properties of the anode surface.

Sulfur poisoning behavior of state-of-the-art anode-supported button cells

Shown in Figure 7 is a picture of the multi-cell testing system built in our lab. The multi-cell system is capable of simultaneously testing 12 button cells under various electrochemical conditions (e.g., potentiostatic, galvanostatic, or potentiodynamic conditions) at a temperature up to 1050 ^oC. The gas distribution system can delivery gas mixtures from humidified inert gas (e.g., N_2), fuel (e.g., H_2), and H_2S containing fuels. It can supply up to four different fuel mixtures with H_2S concentration varying from 0.05 to 100 ppm.

LSM and LSCF based cathodes

The results of the multi-cell testing indicated that the sulfur poisoning behavior for anode-supported cells are similar to that observed for electrolyte-supported cells. Figure 8 shows the results of a multi-cell sulfur poisoning test for ~2000 h using anode-supported cells with a lanthanum strontium manganese oxide (LSM)-based cathode at 750^{o}C under constant current conditions. Similarly, Figure 9 shows the results of another multi-cell sulfur poisoning test (for ~1400 h) at 750^{o}C under constant current conditions using anode-supported cells with a lanthanum strontium cobalt iron oxide (LSCF) cathode. From both experiments, the following observations could be made. First, the relative cell power output drop (in these cases, relative cell voltage drop since the cell currents were kept constant) due to sulfur poisoning increased with H_2S concentration (in terms of pH_2S/pH_2 ratio). Second, the relative cell power output drop increased with current density for the same H_2S concentration under the constant current conditions tested. However, the change in anode resistance due to sulfur poisoning decreased with cell current density. Third, the degree of sulfur poisoning seemed to reach saturation when the pH_2S/pH_2 ratio was low (i.e., 1 ppm). However, there appeared to be a second-stage, continued slower degradation when the pH_2S/pH_2 ratio was 10 ppm and more. This is especially significant for cells with LSCF cathode (see Figure 9): the cell power output continued to degrade in an almost linear fashion for about 1000 h after the initial dramatic drop in performance upon exposure to H_2S (as seen for cells C10 and C12 in Figure 9).

Figure 10 shows some typical impedance spectra of several anode-supported cells with LSCF cathodes in the long-term multi-cell sulfur poisoning experiment at different stages. Like electrolyte-supported cells, the quick cell performance drop upon exposure to H_2S is due to the large increase in the cell (anode) interfacial resistance. It is interesting to note that the so-called 2nd-stage slower degradation, as observed in Figure 9 for cells exposed to 11.8 ppm H_2S, was also due to the continued increase in anode interfacial resistance instead of the change in cell ohmic resistance.

The origin of the observed 2nd-stage sulfur poisoning is not clear at the moment. Such 2nd-stage slower degradation has been observed in several independent studies using different types of cells[8-10]. Since the cell bulk resistance did not change in the 2nd-stage poisoning process and thermodynamic considerations has ruled out the formation of bulk nickel sulfide under the poisoning condition (e.g., 750 ^{o}C, pH_2S/pH_2 = 10 ppm) as the reason for poisoning, the most likely explanation for such behavior (i.e., 2nd-stage slower poisoning) is that it is due to the continued adsorption of sulfur onto the nickel surface towards equilibrium coverage. This is because when the nickel surface is clean, the

sticking coefficient for sulfur adsorption was close to one and remains relatively constant until the surface coverage is close ~0.5-0.6 (i.e., ~50-60% of the area on the surface was covered by sulfur). Beyond that, the sticking coefficient for sulfur adsorption on nickel will decrease by several orders of magnitude[11]. This is expected to significantly lower the rate for the continued adsorption of sulfur onto the nickel surface as the area coverage goes up from ~0.5-0.6 to the ~0.8-0.9 range or even higher. As a result, the observed rate of cell performance degradation decreased dramatically and the poisoning process would last much longer beyond the quick poisoning stage.

Effect of sealant on poisoning behavior

Shown in Figure 11 are the cell voltages for C03 and C04, run in clean hydrogen without exposure to H_2S. Shown in Figures 12 are the cell voltages for cells C05, C06, C07, and C08 before and after the fuel was switched from clean hydrogen to hydrogen containing 0.8 ppm H_2S (at ~600 h). As expected, the cell voltages further decreased when the concentration of H_2S was changed from 0.8 ppm to 1.13 ppm. Shown in Figure 13 are the cell voltages for cells C9, C10, C11, and C12 before and after the fuel was switched from clean hydrogen to hydrogen containing 10 ppm H_2S (at ~300 h).

Summarized in Table 2 and Figure 14 are the cell voltages before and after initial exposure to H_2S. The drop in performance due to initial exposure to H_2S is similar to previous observations: the relative cell power output drop increased with (1) H_2S concentration and (2) cell current density at high concentration of H_2S (under constant current condition). As shown in Table 1 and Figure 14, the drops in performance is much larger for exposure to ~10 ppm H_2S than to ~ 0.8 ppm H_2S regardless of electrochemical testing conditions. However, for cells exposed to ~0.8 ppm H_2S, the observed relative drop in cell voltage was not sensitive to cell operating current density: -7.9% at 200 mA/cm^2, –8.4% (-10.1%) at 400 mA/cm^2, and –8.7% at 600 mA/cm^2. In contrast, for cells exposed to 10 ppm H_2S, the observed relative drop in cell voltage increased with operating current density: –10.5% at 200 mA/cm^2 , -13.1% at 400 mA/cm^2, and –16.7% at 600 mA/cm^2.

Shown in Figure 15 (a) and (b) are normalized changes in cell voltage (in percentage) after the large initial voltage drop due to switching from H_2 to H_2 containing H_2S. For cells subject to 0.8 ppm H_2S, after the initial poisoning effect, the second stage degradation in performance was *not* significant for cells operated at current densities of 200 and 400 mA/cm^2. In contrast, the cell operated at 600 mA/cm^2 experienced a continued drop in performance during the entire duration of the testing; but the degradation rate seems to be much lower than that observed for the cells sealed using an Aremco sealant under similar testing conditions. However, the cell degraded rapidly when the

concentration of H_2S was switched from 0.8 ppm to 1.13 ppm. Third, for the cells exposed to 10 ppm H_2S, after the initial performance drop due to sulfur poisoning, the second stage degradation in performance was significant for the cells operated at 600 mA/cm^2 , but *not* significant for the cells operated at 200 and 400 mA/cm^2, similar to that observed for the cells exposed to 1 ppm H_2S. The second stage degradation for the cells operated at 600 mA/cm^2 (exposed to ~1 and 10 ppm H_2S) may be attributed to either a second stage sulfur poisoning or a degradation of cathode performance at a high operating current density.

CONCLUSIONS

Under the support of this SECA project, we made important progress in elucidation of the mechanism of sulfur poisoning of Ni-YSZ anode materials and development of modified anodes with enhanced sulfur tolerance. The following significant conclusions can be drawn from the work completed in this project:

- The sulfur poisoning and recovery for Ni-YSZ anode of SOFC is strongly influenced by operating parameters such as temperature, H_2S concentration, and cell current density/voltage. Generally, sulfur poisoning is more severe at lower temperature, higher H_2S concentration or lower cell current density (higher cell voltage).
- The *in-situ* Raman spectroscopy experiment suggests that sulfur poisoning is not likely to be caused by formation of conventional sulfide. However, bulk sulfides do form at lower temperature (<400 ^{o}C) in fuels with H_2S in the ppm range, also causing dramatic morphology changes at the Ni surface. The vibrations at the Γ-point of the sulfides are computed and confirmed with Raman measurements.
- The effective operational windows have been identified from the computed Ni-S phase diagram, which can distinguish the clean Ni surface, the Ni surfaces partially covered with adsorbed sulfur atoms, and bulk nickel sulfide Ni_3S_2.
- Quantum chemical calculations suggest that some metals such as Ag, Cu and Mo have lower sulfur adsorption energy and are potential candidate materials for sulfur resistant anodes for SOFCs.
- The Nb_2O_5 coated Ni-YSZ anode showed promising sulfur tolerance in 50-ppm H_2S contaminated fuels. Analysis of niobium oxide indicated that the enhanced sulfur tolerance for niobium oxide coated Ni-YSZ anode is due to transformation of the niobium oxide to corresponding niobium sulfides in sulfur containing fuels.

- A multi-cell testing system has been built: it enables simultaneous testing of up to 12 cells and can greatly increase the experiment output. The initial sulfur poisoning behavior of state-of-the-art anode-supported SOFC button cells are similar to that of the electrolyte-supported cells. The observed relative cell power output drop increased with H_2S concentration and with cell current density under the constant current conditions. However, the long-term sulfur poisoning behavior of those cells indicate that there might be a second-stage slower degradation due to sulfur poisoning, which would last for a thousand hour or even longer.
- When sealant was changed from Aremco sealant (Ceramabond® 552VFG) to G-18 glass sealant (from PNNL), the 2nd stage performance remained relatively constant for continuous operation up to ~3,000 hours at 200 and 400 mA/cm^2. For cells operated at 600 mA/cm^2, however, there appears a continued degradation in performance after the *initial* large drop in performance due to the H_2S exposure, but at a much lower rate.

TABLES

Table 1. Vibrational frequencies (cm^{-1}) determined by theoretical calculations and Raman measurements for Ni_3S_2, NiS, Ni_3S_4 and NiS_2.

Material	Modes	Calc.	Expt.
Ni_3S_2	E(1)	367, 367	351
	$A_1(1)$	320	325
	E(2)	317, 316	303
	E(3)	241, 241	223
	E(4)	204, 203	201
	$A_1(2)$	201	189
NiS	$A_1(1)$	356	370
	E(1)	341, 341	349
	$A_1(2)$	290	300
	$A_1(3)$	254	
	E(2)	252, 251	246
	E(3)	231, 230	
	E(4)	201, 201	
	E(5)	148, 148	
Ni_3S_4	$A_{1g}(1)$	388	375
	$T_{2g}(1)$	339, 338, 338	335
	$T_{2g}(2)$	284, 284, 283	285
	$E_g(1)$	208, 207	222
	$T_{2g}(3)$	206, 206, 205	
NiS_2	$T_g(1)$	462, 462, 461	489
	$A_g(1)$	446	479
	$T_g(2)$	342, 341, 341	
	$E_g(1)$	285, 285	285
	$T_g(3)$	278, 278, 277	273

Table 2. Cell Voltages before and after initial exposure to H_2S

Cell No.	pH_2S/H_2 (ppm)	Current density (mA/cm^2)	Cell Voltage (mV) before exposure to H_2S	Cell Voltage (mV) after exposure to H_2S	Percentage of voltage drop (%)
1	0	600	738	NA	NA
2	0	Cell failed	NA	NA	NA
3	0	200	880	NA	NA
4	0	400	829	NA	NA
5	1	200	935	861	7.9%
6	1	400	858	771	10.1%
7	1	600	719	656	8.7%
8	1	400	833	763	8.4%
9	10	400	851	739	13.1%
10	10	400	833	715	14.1%
11	10	200	917	821	10.5%
12	10	600	762	635	16.7%

FIGURES

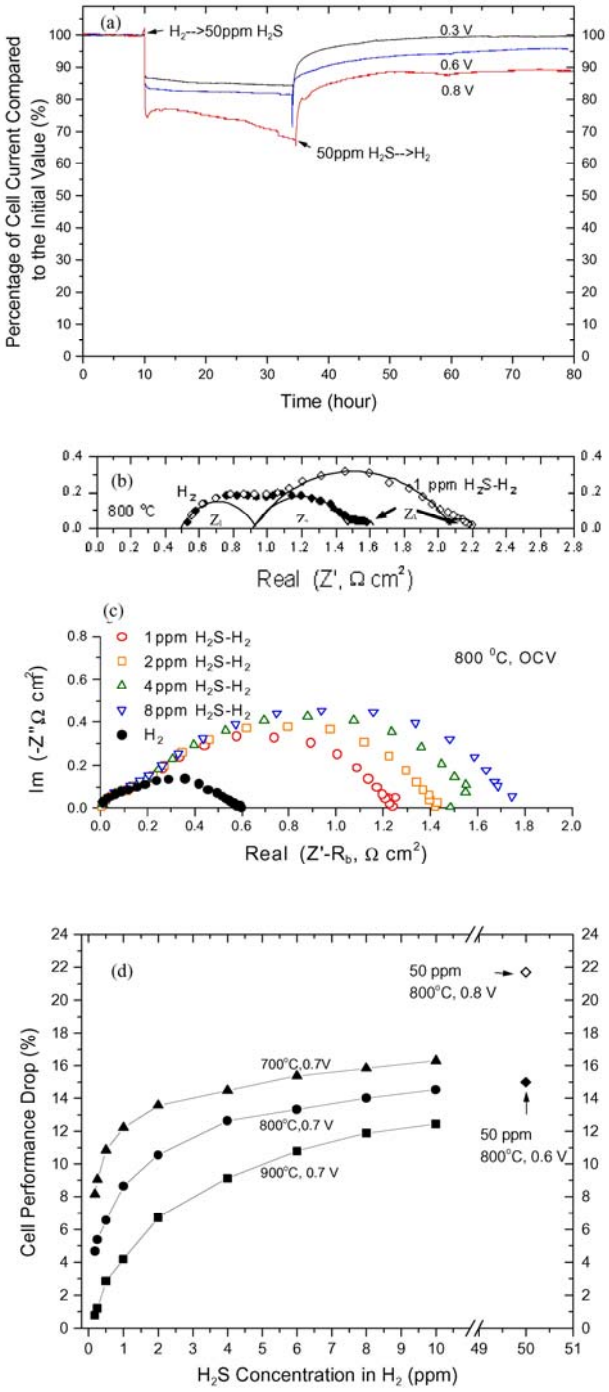

Figure 1. (a) Influence of cell voltage on sulfur poisoning and regeneration for Ni-YSZ cermet anode at 800 ^{o}C; (b) change in impedance spectrum for a cell measured at OCVs using 2-electrode configuration in fuels with and without 1 ppm H_2S; (c) change in impedance spectrum for the anode/electrolyte interface measured at OCV using 3-electrode configuration in fuels with different concentration of H_2S; (d) influence of H_2S concentration on the extent of sulfur poisoning for Ni-YSZ anode at different temperatures.

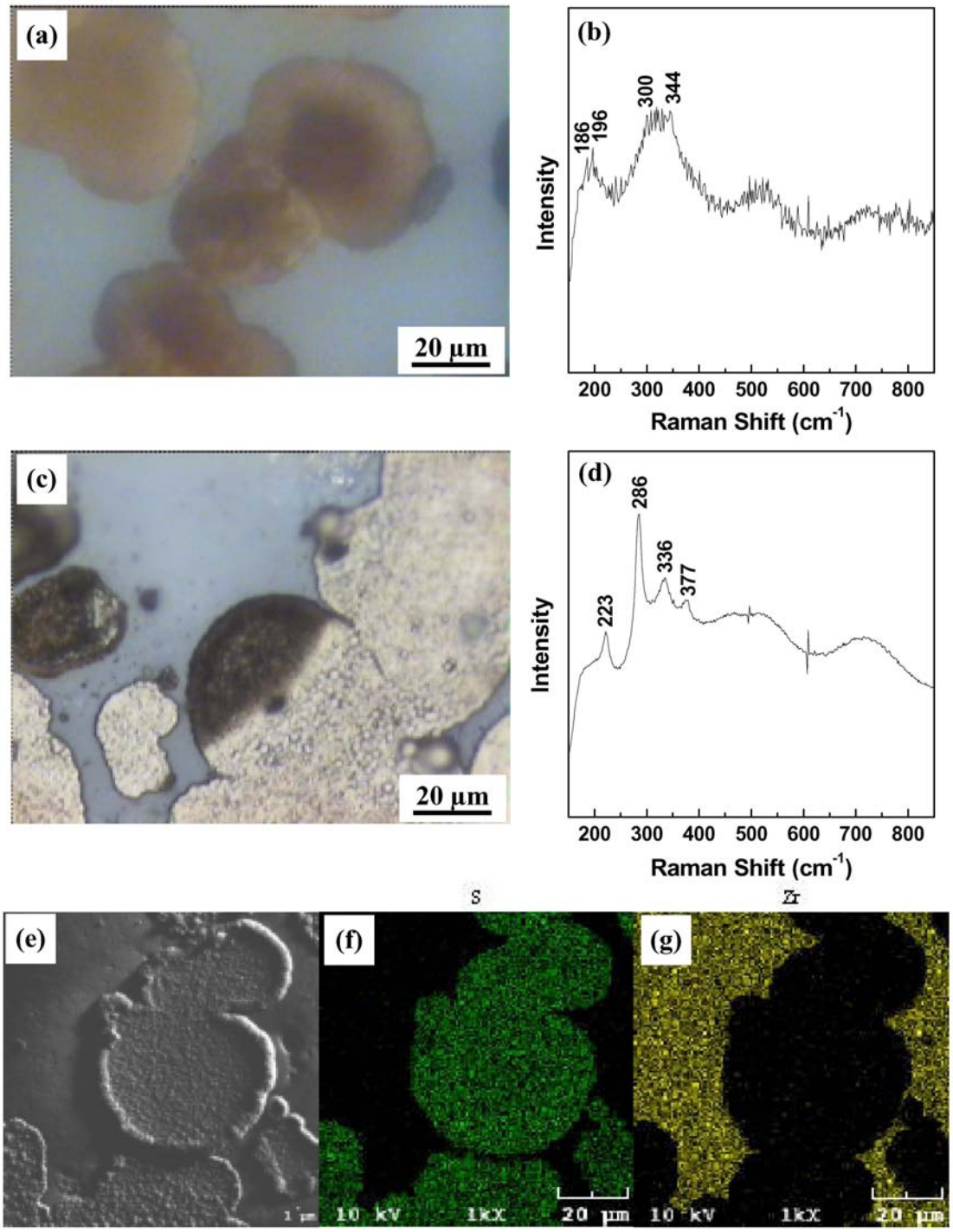

Figure 2. Optical microscopy image (a) and corresponding Raman spectrum from the Ni region (b) for the Ni-YSZ composite in in-situ Raman experiment at 216 ^{o}C in a fuel with 50 ppm H_2S; optical microscopy image (c), corresponding Raman spectrum taken from the Ni region (d), SEM image (e), S elemental map (f) and Zr element map (g) for the Ni-YSZ composite heated treated at 600 ^{o}C in 50 ppm H_2S/50% H_2/1.5% H_2O/48.5%N_2 for 20 h.

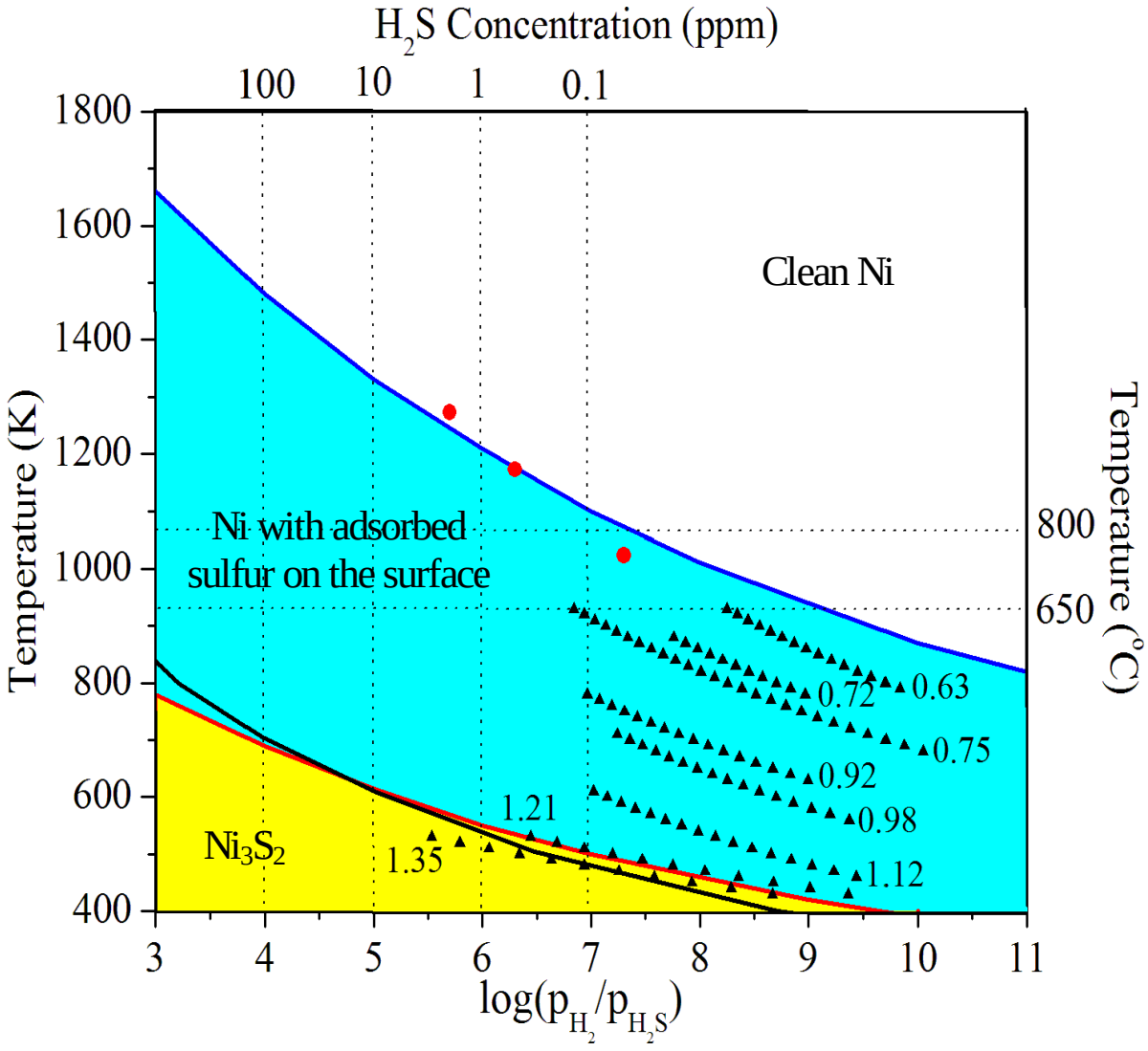

Figure 3. Calculated phase diagram for the S-Ni system in H_2S/H_2 fuel mixtures. The white, blue, and yellow regions represent clean Ni phase without adsorbed sulfur on the surface, Ni phase with adsorbed sulfur on the surface, and Ni_3S_2 bulk phase, respectively. The blue line is the calculated phase boundary between clean Ni surface and Ni surface with adsorbed sulfur; the red line is the calculated phase boundary between Ni surface with adsorbed sulfur and Ni_3S_2 bulk phase; the black line is phase boundary between bulk nickel and Ni_3S_2 determined by experiments (1). The black triangles are data points for the sulfur chemisorption isosteres on Ni surface with different surface coverage (3). The red circles represent the experimentally determined critical H_2S concentration values above which the sulfur poisoning of fuel cell anode became significant (2).

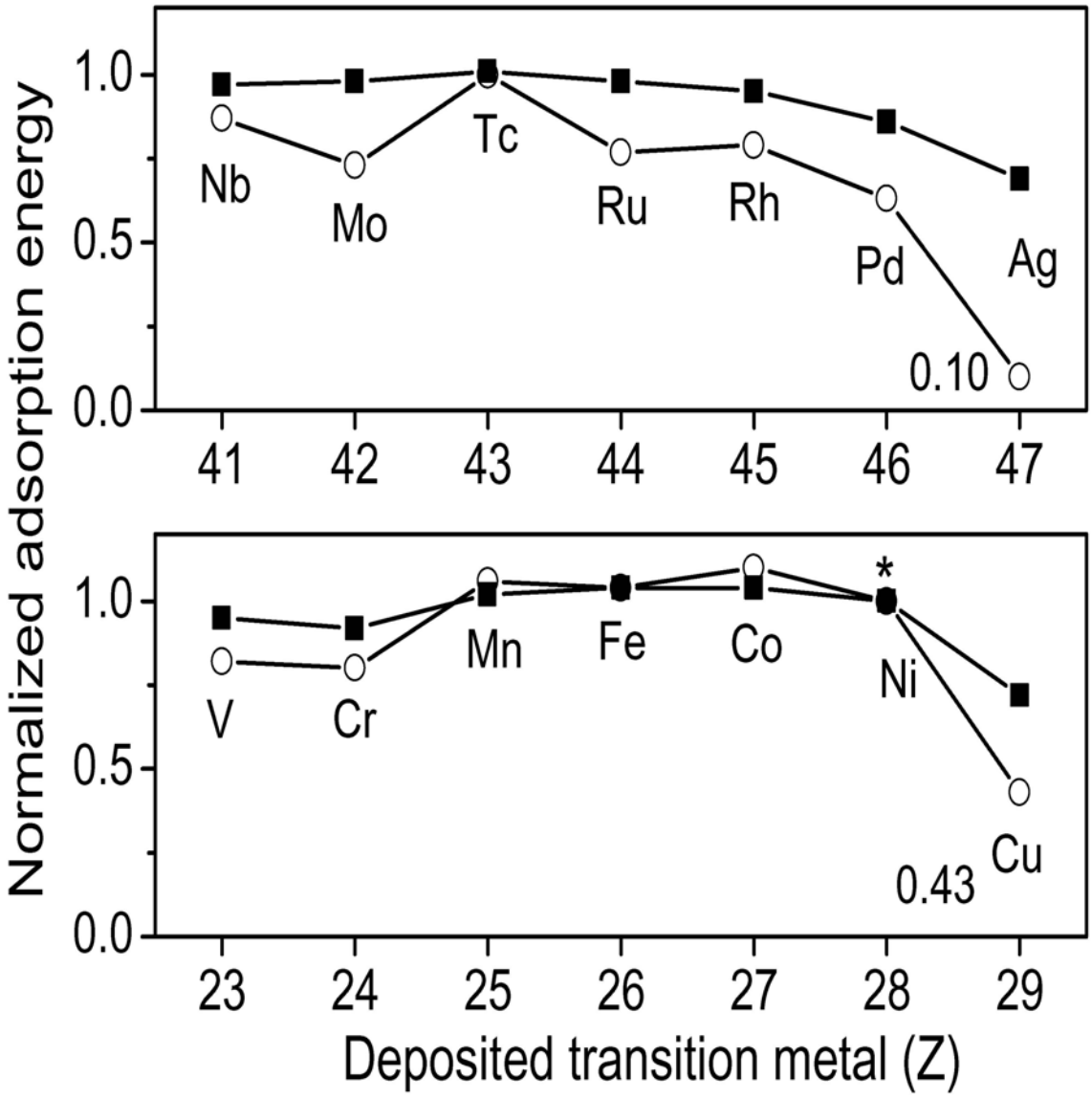

Figure 4. Comparison of predicted molecular adsorption energies for H_2S (open circle) and dissociative adsorption energies for H_2 (closed square) on modified Ni.

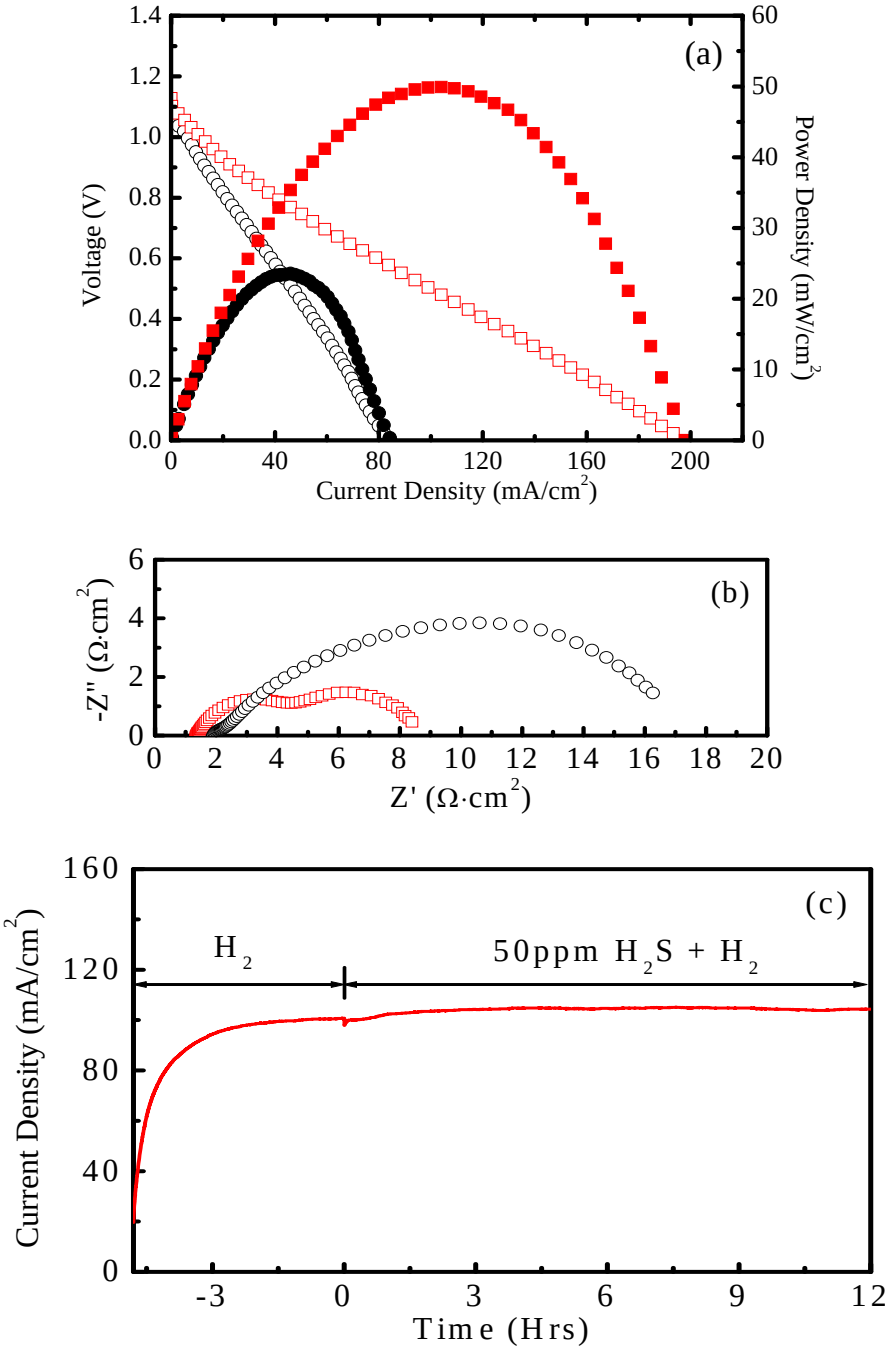

Figure 5. (a) Current-voltage relationship and power output and (b) impedance spectra for cells (Pt/YSZ/dense Ni-YSZ tri-layer structure) with (squares in red) and without (circles in black) Nb_2O_5 coating in dry H_2 at 700 °C, and (c) the change in current density for the cell with a Nb_2O_5 coating over the dense Ni-YSZ anode in dry 50 ppm H_2S balanced with H_2 at 700 ºC.

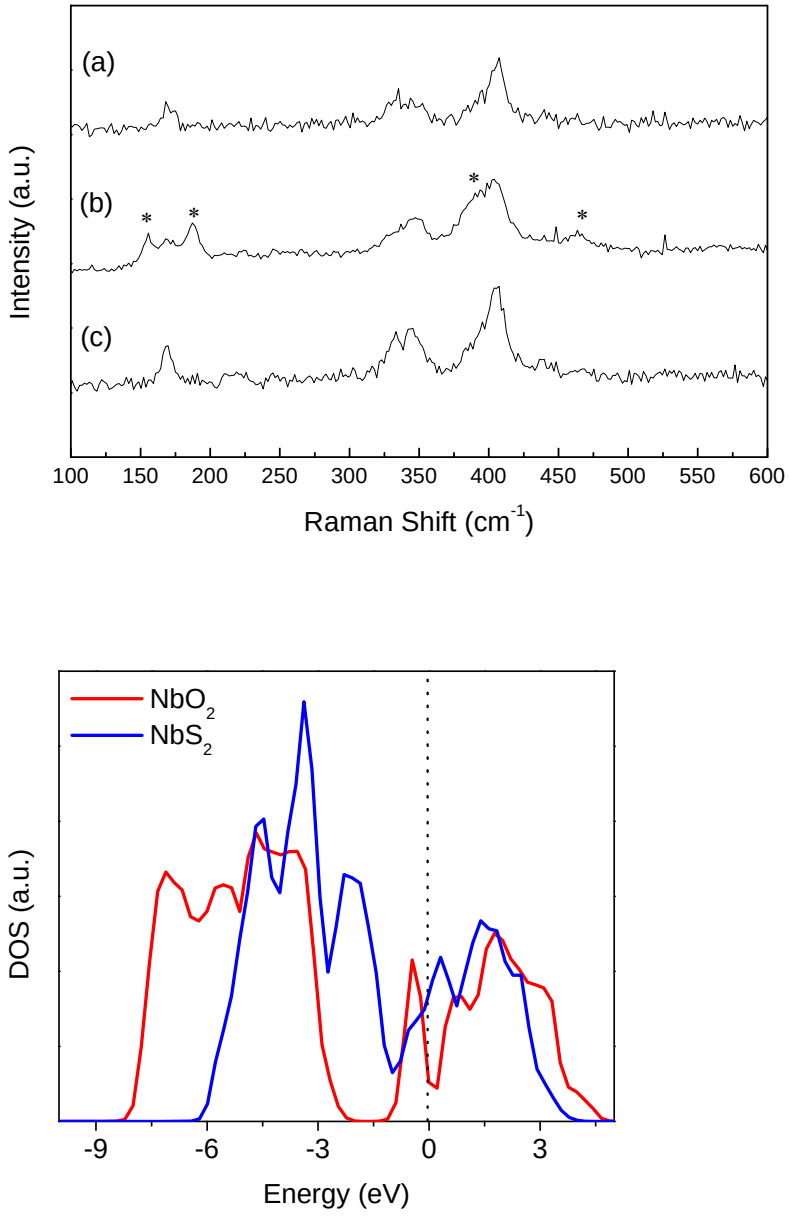

Figure 6. (a) Raman spectrum of NbO_2 powder after reduction in H_2 at 800 ^oC for 24 h. (b) Raman spectrum of NbO_2 powder after being exposed to 100 ppm H_2S balanced with H_2 at 700 ^oC for 15 h; the asterisk represents the newly emerged peaks that correspond to NbS_2. (c) Raman spectrum of Nb_2O_5 powder after regeneration in H_2. (d) DOS analysis for NbO_2 and NbS_2.

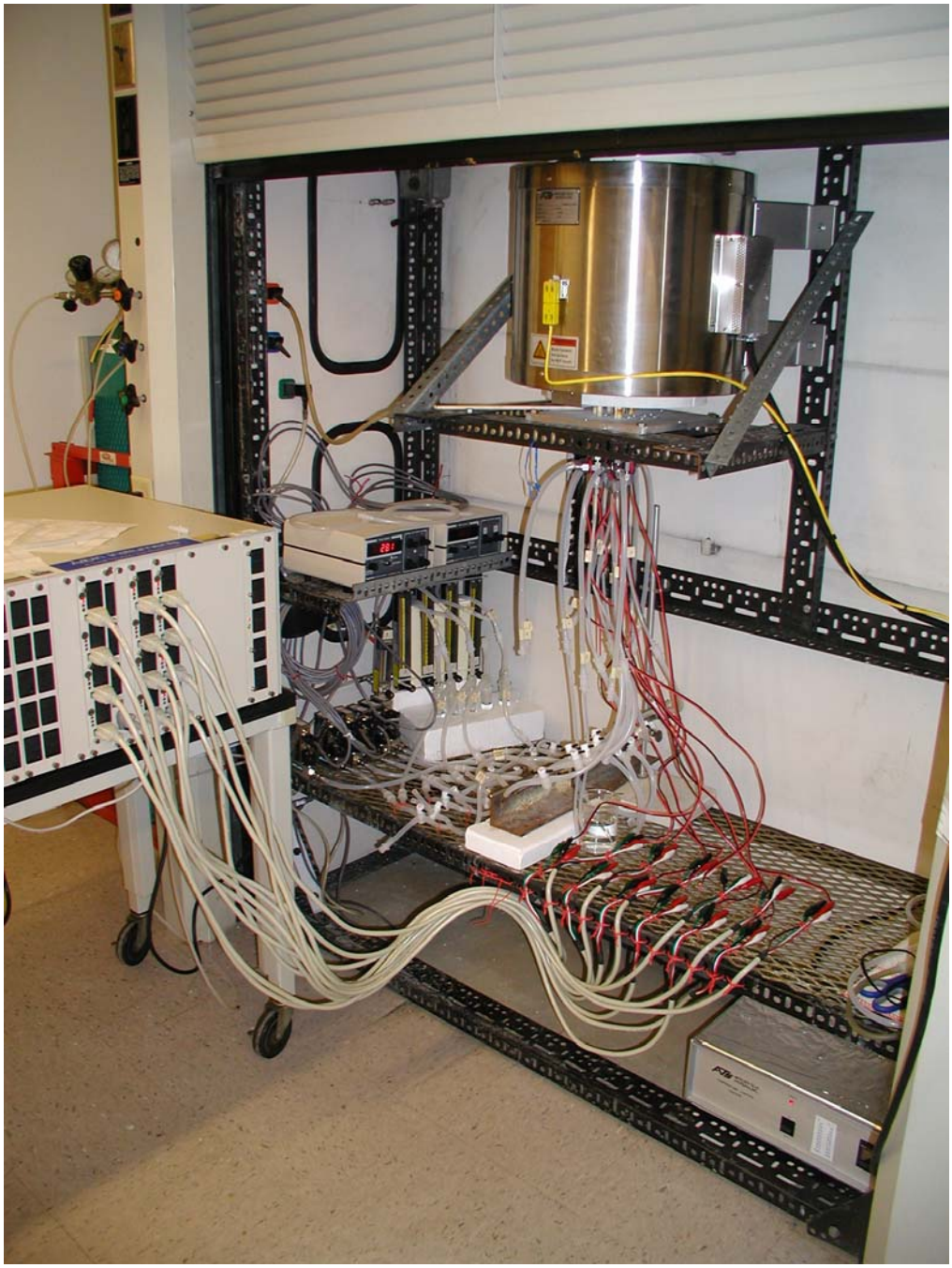

Figure 7. The multi-cell testing system consisting of a high temperature furnace, a gas distribution system, and a 12-channel electrochemical testing system.

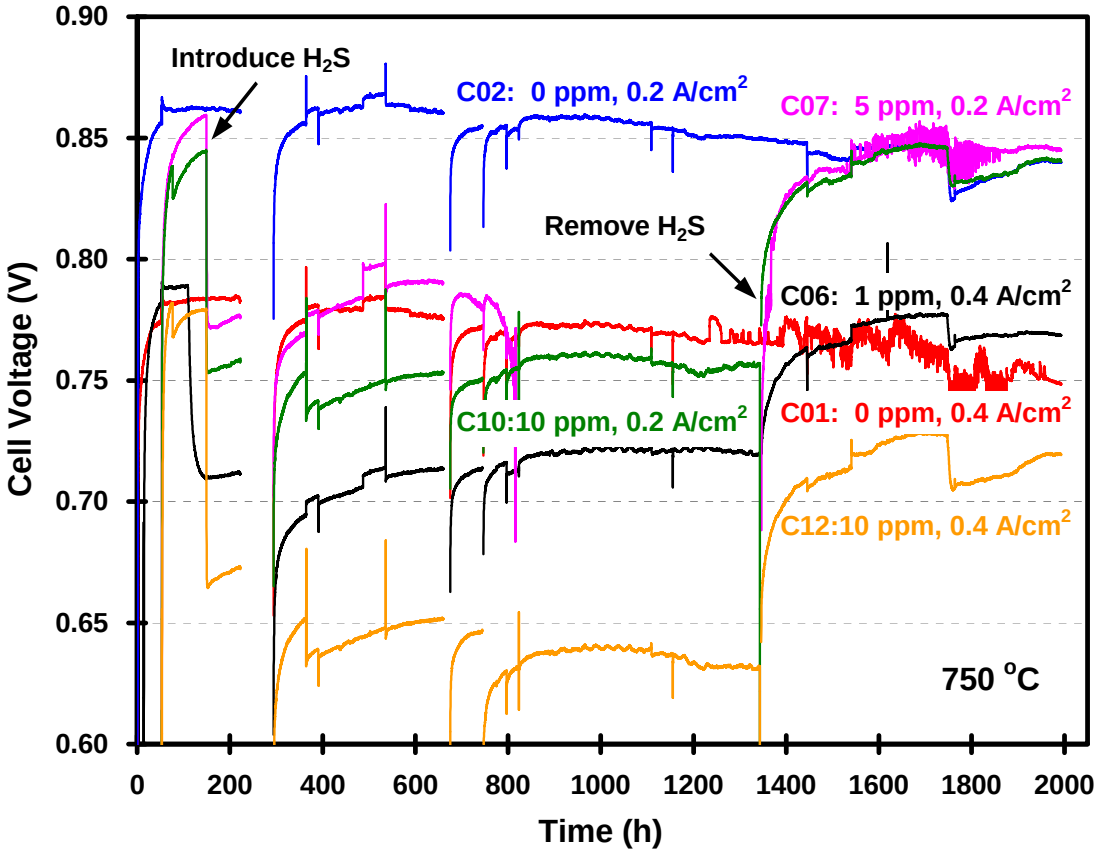

Figure 8. Plots of cell voltage versus time for a long-term multi-cell sulfur poisoning experiment using anode-supported cells with an LSM-based cathode at 750 °C under constant current conditions. The pH_2S/pH_2 ratios were 0, 1, 5, and 10 ppm, and the current densities were 0.2 and 0.4 A/cm^2.

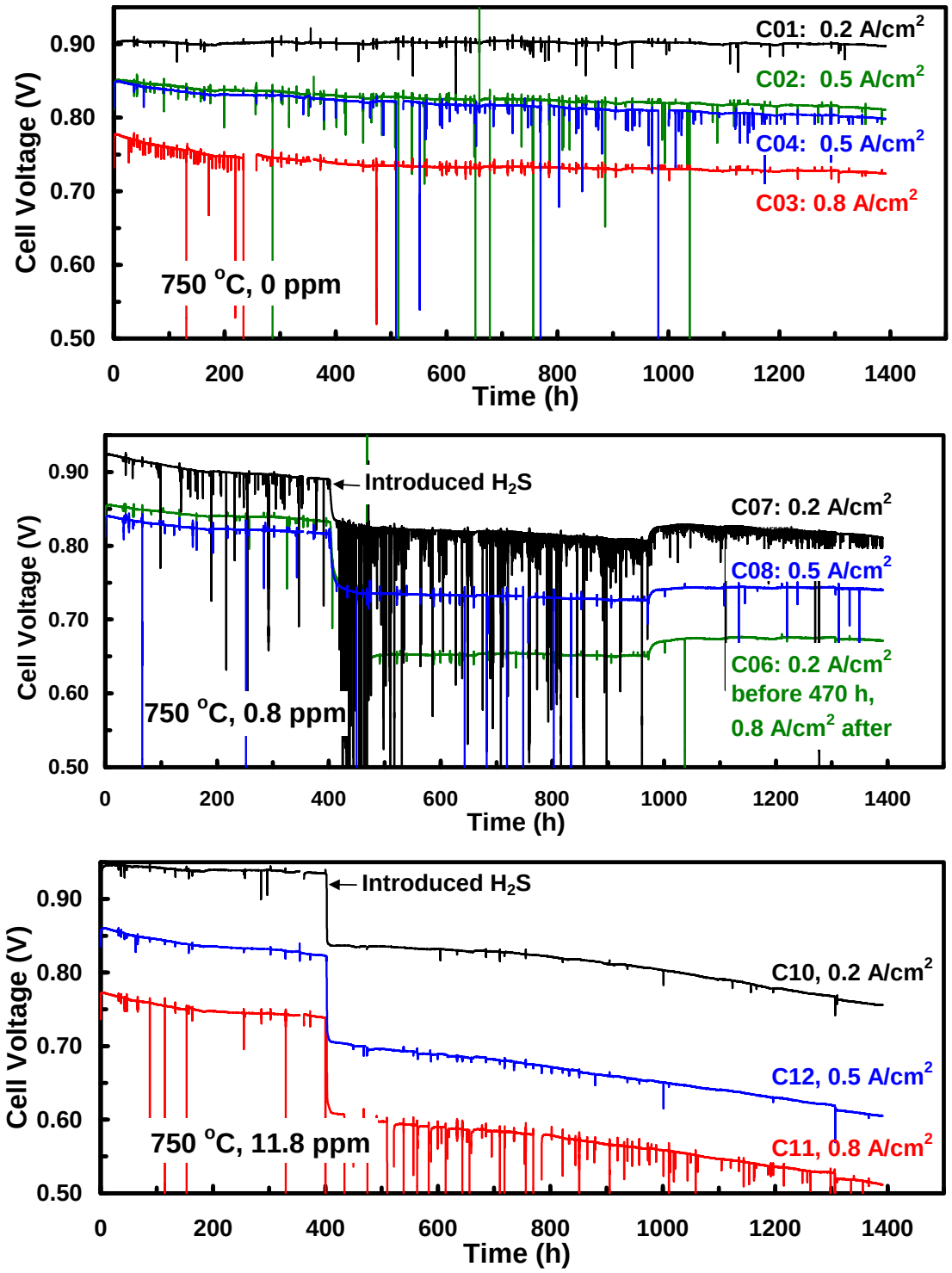

Figure 9. Plots of cell voltage versus time for a long-term multi-cell sulfur poisoning experiment using anode-supported cells with an LSCF-based cathode at 750 °C under constant current conditions. The pH_2S/pH_2 ratios were 0, 0.8, and 11.8 ppm, and the current densities were 0.2, 0.5, and 0.8 A/cm^2.

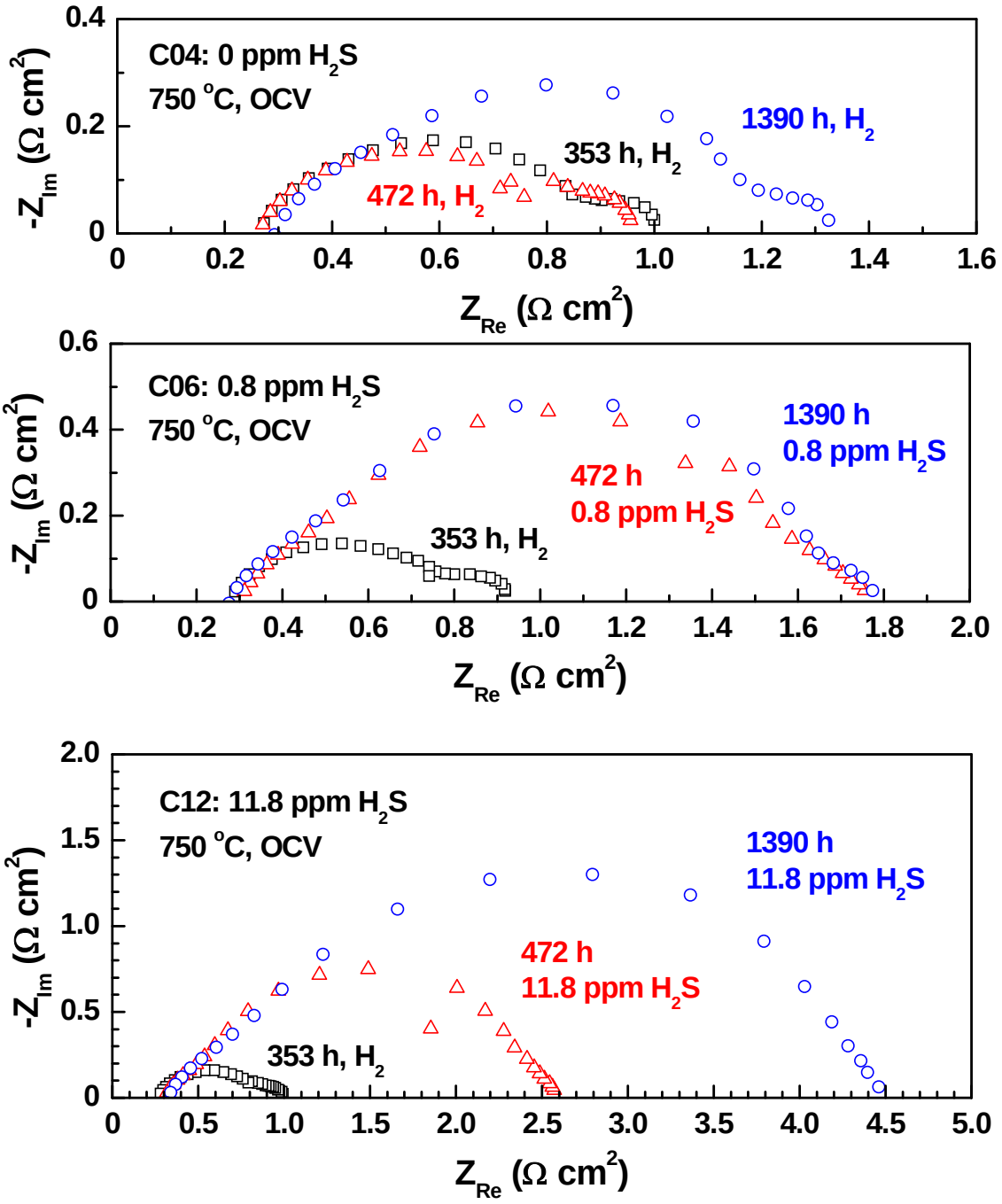

Figure 10. Full cell impedance spectra at 750 °C under open circuit condition for cells C04, C06, and C12 at different stages in the long-term sulfur poisoning experiment shown in Figure 2. Note that 353 h was before the introduction of H_2S, 472 h was after the quick poisoning stage finished, and 1390 h was after the cells were subject to H_2S for ~1000 h.

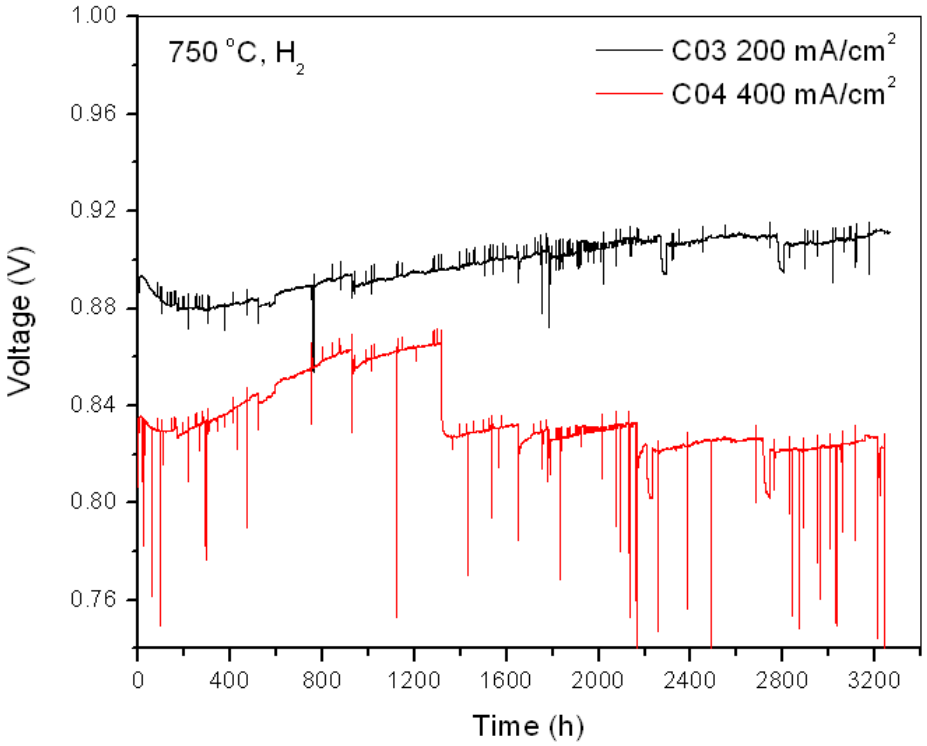

Figure 11. The performances of the cells without exposure to H_2S.

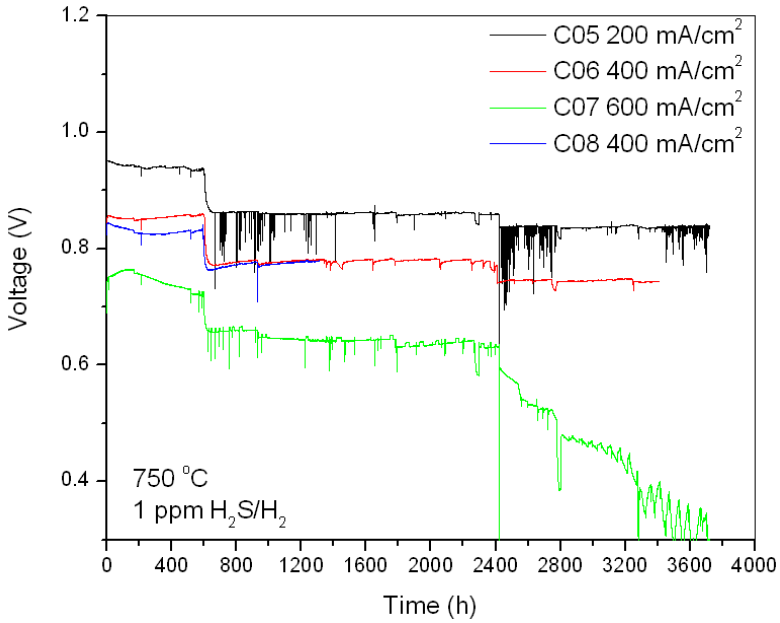

Figure 12. Performances of the cells operated at 200, 400, and 600 mA/cm^2 and exposed to 0.8 ppm H_2S after operation in hydrogen for ~ 600 h. The concentration of H_2S was changed from 0.8 ppm to 1.13 ppm at ~ 2400 h (change of gas cylinder); the effect of H_2S concentration is clearly seen.

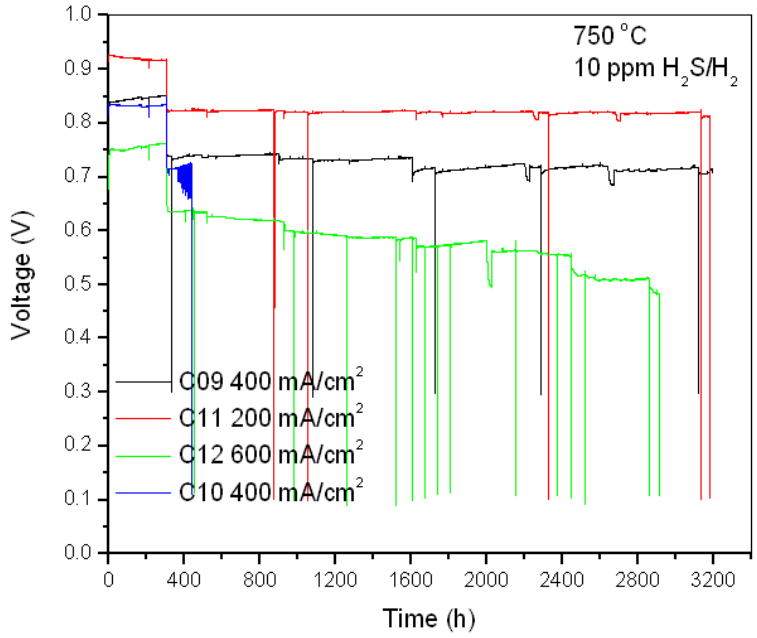

Figure 13. Performances of the cells operated at 200, 400, and 600 mA/cm^2 and exposed to 10 ppm H_2S after operation in clean hydrogen for ~300 hours (not shown in the figure). It appears that there is no second stage sulfur poisoning effect for the cells operated at 200 and 400 mA/cm^2. However, the degradation in performance seems to be significant for the cell operated at 600 mA/cm^2, due to either a second stage sulfur poisoning effect of the anode or degradation of the cathode.

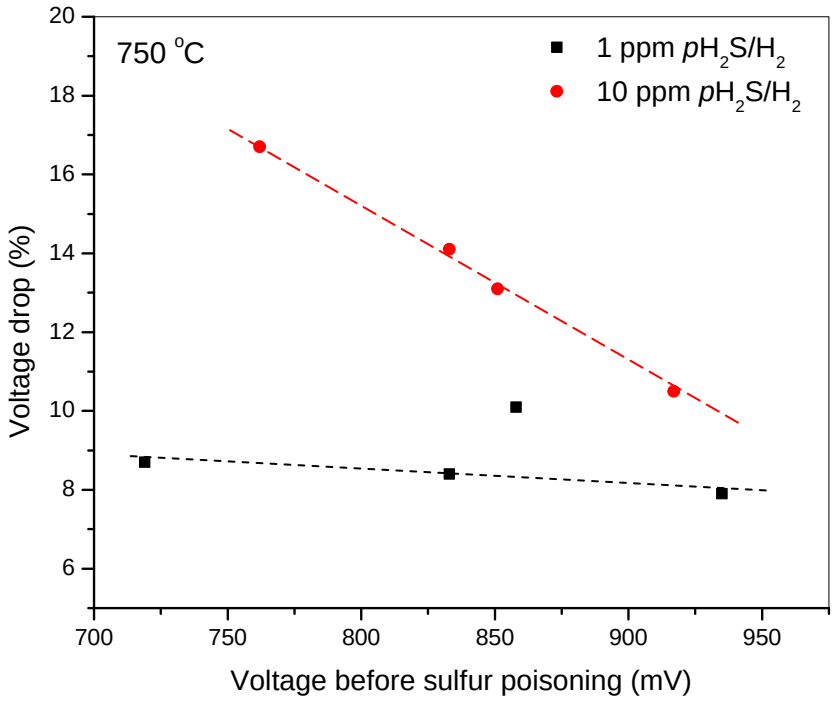

Figure 14. Cell voltage drop upon initial exposure to H_2 containing 1 and 10 ppm H_2S.

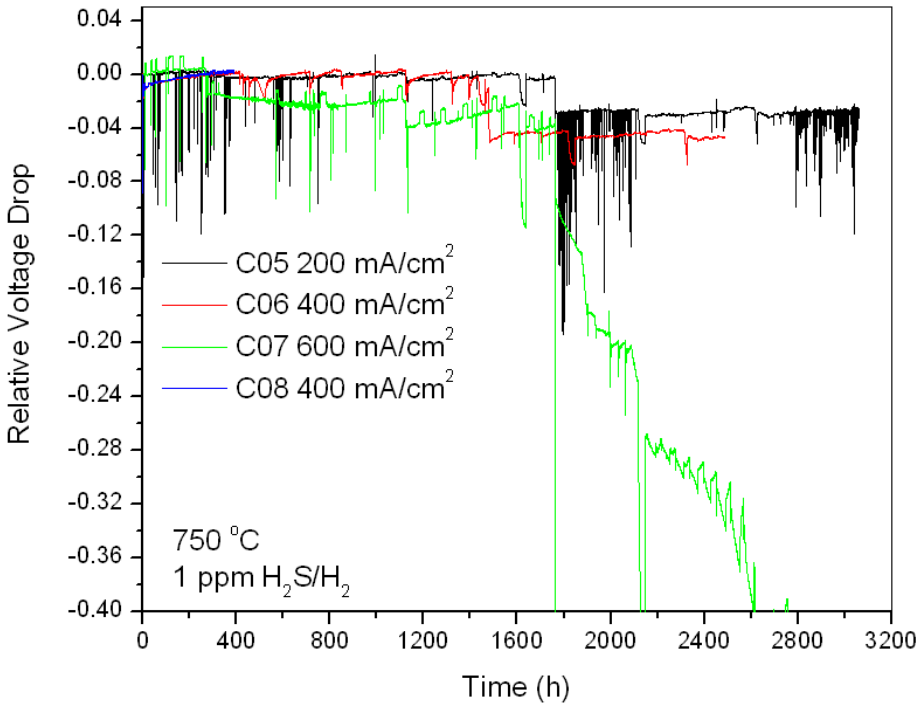

(a)

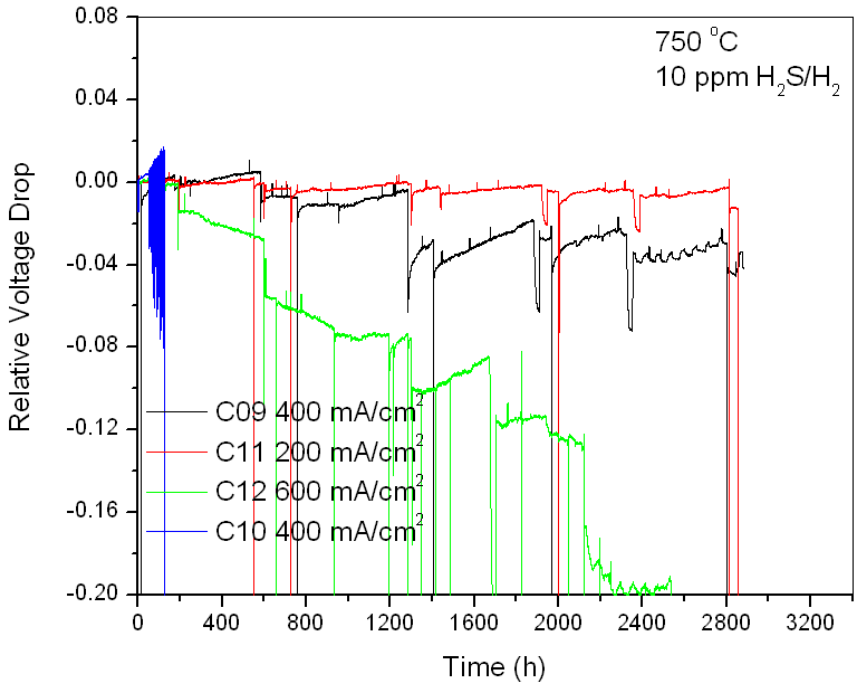

(b)

Figure 15. Normalized voltage changes (in percentage) after the large initial voltage drop due to switching from clean H_2 to H_2 containing (a) 1 ppm and (b) 10 ppm H_2S. A reading of -0.01 on the vertical axis would be equivalent to 1% voltage drop, corresponding to a second stage degradation due to sulfur poisoning.

REFERENCES

[1] N. Q. Minh, Ceramic fuel cells. Journal of the American Ceramic Society**,** 1993, 76,563.

[2] B.C.H. Steele, A. Heinzel, Materials for fuel-cell technologies , Nature 2001, 414, 345.

[3] L Yang, CD Zuo, S Wang, et al. A novel composite cathode for low-temperature SOFCs based on oxide proton conductors. Advanced Materials, 2008, 20: 3280

[4] Y. M. Choi, C. Compson, Charles, M. C. Lin, M. Liu, "A mechanistic study of H_2S decomposition on Ni- and Cu-based anode surfaces in a solid oxide fuel cell," Chemical Physics Letters, 421, 179-183 (2006).

[5] T Rosenqvist: J. Iron Steel Inst. 176 (1954) 37.

[6] Y Matsuzaki, I Yasuda: The poisoning effect of sulfur-containing impurity gas on a SOFC anod: Part I. Dependence on temperature, time and impurity concentration. Solid State Ionics 132 (2000) 261.

[7] JG McCarty, H Wise: Thermodynamics of sulfur chemisorption on metals. I. Alumina-supported nickel. J. Chem. Phys. 72 (1980) 6332.

[8] S Zha, Z Cheng, M Liu, "Sulfur poisoning and regeneration of Ni-based anodes in solid oxide fuel cells." Journal of the Electrochemical Society 154 (2007) B201-B06.

[9] JP Trembly, AI Marquez, TR Ohrn, DJ Bayless, "Effects of coal syngas and H2S on the performance of solid oxide fuel cells: Single-cell tests." Journal of Power Sources 158 (2006) 263-73.

[10] ER Ray, "Contaminant Effects in Solid Oxide Fuel Cells," in W.J. Hubner (Ed.), Proceedings of the Third Annual Fuel Cells Contractors Review Meeting. U.S. Department of Energy, Washington, DC, 1992, p. 108-16.

[11] CH Bartholomew, PK Agrawal, JR Katzer, "Sulfur Poisoning of Metals." Advances in Catalysis 31 (1982) 153.